Orchestrating Improbable Chemistries: Structural Snapshots of B_{12}-Dependent Methionine Synthase's Catalytic Choreography

Johnny Mendoza[1‡], Kazuhiro Yamada[1,2‡†*], Carmen Castillo[3], Catherine A. Wilhelm[1§], Markos Koutmos[1,2,3*]

[1]Department of Chemistry, University of Michigan, Ann Arbor, MI, 48109
[2]Program in Biophysics, University of Michigan, Ann Arbor, MI, 48109
[3] Department of Biological Chemistry, University of Michigan, Ann Arbor, MI, 48109
‡Johnny Mendoza and Kazuhiro Yamada contributed equally to this work
†Current Address: Department of Biological Chemistry, University of Michigan, Ann Arbor, MI, 48109
§Current Address: Department of Chemistry, Wayne State University, Detroit, MI, 48202
*To whom correspondence should be addressed: yamadak@umich.edu (co-corresponding), mkoutmos@umich.edu (corresponding)

Abstract

Cobalamin (vitamin B_{12}) and its derivatives are used to power chemical transformations crucial for life. Among these essential reactivities are methylations, of which cobalamin-dependent methionine synthase (MS) is the canonical example. MS catalyzes three distinct methyl transfers central to one-carbon metabolism. Despite its importance in the biological methyl cycle and relevance to human health, fundamental studies on the molecular basis of MS catalysis have proven elusive due to substantial biochemical challenges associated with MS from traditional sources. Here, we leverage our previously established thermophilic model system (*t*MS), its remarkable stability, and its ability to bind non-native cobalamin cofactors to systematically capture previously unattainable conformations via crystallography, presenting the first structures of a cobalamin enzyme in action (folate demethylation and homocysteine methylation). We establish the role of the folate (Fol) domain and its associated linkers in triggering the structural transitions required for activity. Our work highlights the importance of linkers in mediating large-scale rearrangements that underpin the catalysis of improbable chemistries. By providing the first structural blueprints associated with two cobalamin-mediated methyl transfers, we lay the groundwork for exploring cobalamin's biocatalytic potential and provide a framework by which Nature harnesses dynamic motions to achieve dynamic chemical outcomes.

Main

Methionine synthase is a multi-modular enzyme capable of binding and activating three substrates (homocysteine, HCY; methyltetrahydrofolate, MTF/folate, FOL; and *S*-adenosylmethionine, SAM) to achieve three distinct methylations (Reaction I, II, and III, Fig. 1a). Reactivity is governed by access to the cobalamin cofactor and its oxidation state, with each reaction associated with the formation of three different catalytically competent ternary complexes and an active site between the Cob domain and its respective substrate domain (Fig. 1a)[1]. The cobalamin cofactor's oxidation state alternates between Co(III) and Co(I) states during the catalytic cycle (Reaction I and II, Fig. 1a) but the highly reactive Co(I) is oxidized to the catalytically inactive Co(II) once every 2000 turnovers[2,3]; MS can restore catalytic competency

by entering the reactivation cycle, during which reductive methylation of Co(II) regenerates the catalytically competent Co(III) state, allowing for re-entry to the catalytic cycle (Reaction III, Fig. 1a)[3,4]. However, while rich biochemical studies exist on factors that govern and can trigger MS domain rearrangements, atomic level insights into what the conformations associated with the catalytic cycle look like has eluded structural characterization[5,6,7,8].

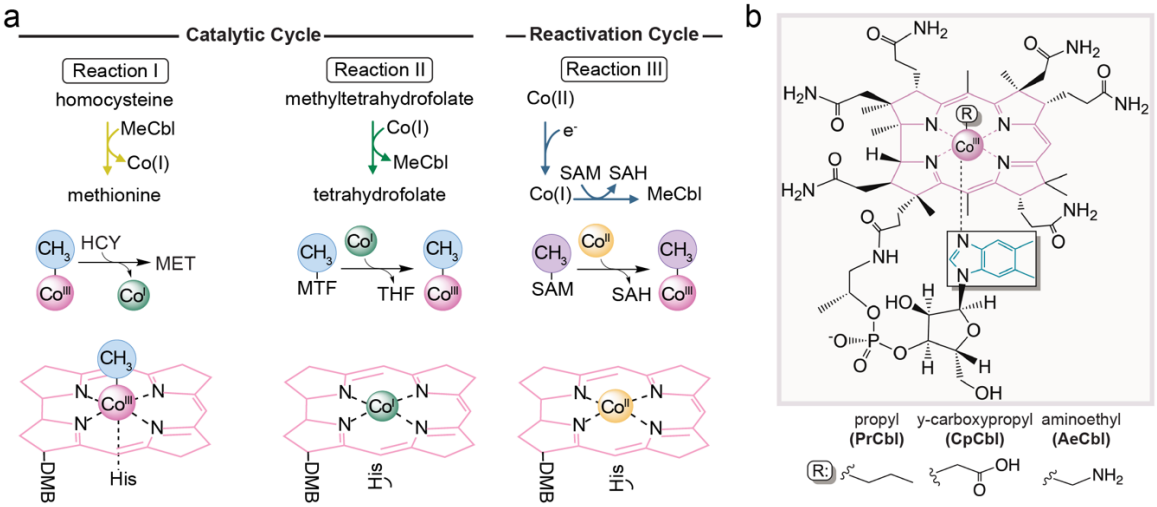

Figure 1. Methionine synthase harnesses its cobalamin cofactor to dictate chemical outcome. **a** The three distinct methyl transferase reactions catalyzed by methionine synthase (MS). The primary catalytic cycle allows for the cobalamin cofactor to alternate between the Co(III) and Co(I) states for homocysteine methylation (Reaction I) and folate demethylation (Reaction II), respectively. Due to the microaerophilic conditions present in vivo, MS can undergo inactivation when Co(I) is oxidized to the inactive Co(II) state. During the reactivation cycle, the active state of the cofactor is restored via reductive methylation with SAM/AdoMet, regenerating the Co(III) state and allowing for re-entry to the catalytic cycle (Reaction III). The coordination number, redox state, and His ligation status are particular to each methylation. **b** The native cobalamin cofactor used by methionine synthase is methylcob(III)alamin. Synthetic cobalamin cofactors incapable of catalysis can and have been used to modulate function via cofactor mimicry and subsequent inhibition and can capture distinct conformations.

Previously, we used a thermophilic MS homolog (*t*MS) from *Thermus thermophilus* that displayed robust stability, allowing for exhaustive functional mutagenesis studies, purification as an apoenzyme, and facile reconstitution with non-native cobalamin cofactors to form novel holoenzymes (Fig. 1b)[9]. This model system allowed for the determination of the first full-length structure of MS (8SSC) captured via crystallography and the observation of holoenzyme formation *in crystallo* (8SSD, 8SSE)[9]. The ability to purify excised domain constructs, coupled with the ability to purify all mutants generated, allowed us to begin interrogating MS mechanistically using a combination of rationally chosen non-native cobalamins and *t*MS constructs[9].

Here, we leverage our *t*MS model to capture five new crystal structures of MS in action, three pre-catalytic conformations and two catalytically competent conformations, that provide insights into the structural motifs used to guide and gate the large conformational rearrangements required for MS catalysis. We show that the MS conformational ensemble is more expansive than previously appreciated, adopting additional pre-catalytic conformations[10,11] (Cap-on) that

highlight the role of the Fol:Cap linker (Linker II, Fig. 2) in mediating structural transitions, where it acts as a hinge. The structures show that the “uncapping” transition required for cobalamin access (Cap:Cob linker, Linker III, Figs. 2b, c, and d) is predetermined, adopting the same placement relative to the Cob domain in all observed Cap-off structures. The two catalytic conformations (Fol-on, Reaction II; Hcy-on, Reaction I, Fig. 2b) provide the first structural blueprints of a B_{12}-dependent methyltransferase active site, one required for folate demethylation and the other for homocysteine methylation. Our biochemical data highlight the role the Fol domain plays in steering the conformational ensemble towards catalytic states, while also demonstrating that the cobalamin cofactor adopts a His-off, five-coordinate state during catalysis. Notably, we demonstrate the importance of the ligating His residue in signaling and guiding the conformational ensemble, positing that His-on ligation gates the ensemble into Cap-on states (pre-catalytic), enabling MS to ‘reset’ and interconvert between these states, and His-off ligation allows for cobalamin flexibility and substrate domain access after uncapping (Cap-off, catalytic/reactive). We propose a revised mechanistic and structural model for MS, one that emphasizes the role of a linker (Fol:Cap, Linker II), His-off ligation, and guided domain uncapping in gating and thereafter guiding rearrangements that allow for cofactor access required for catalysis.

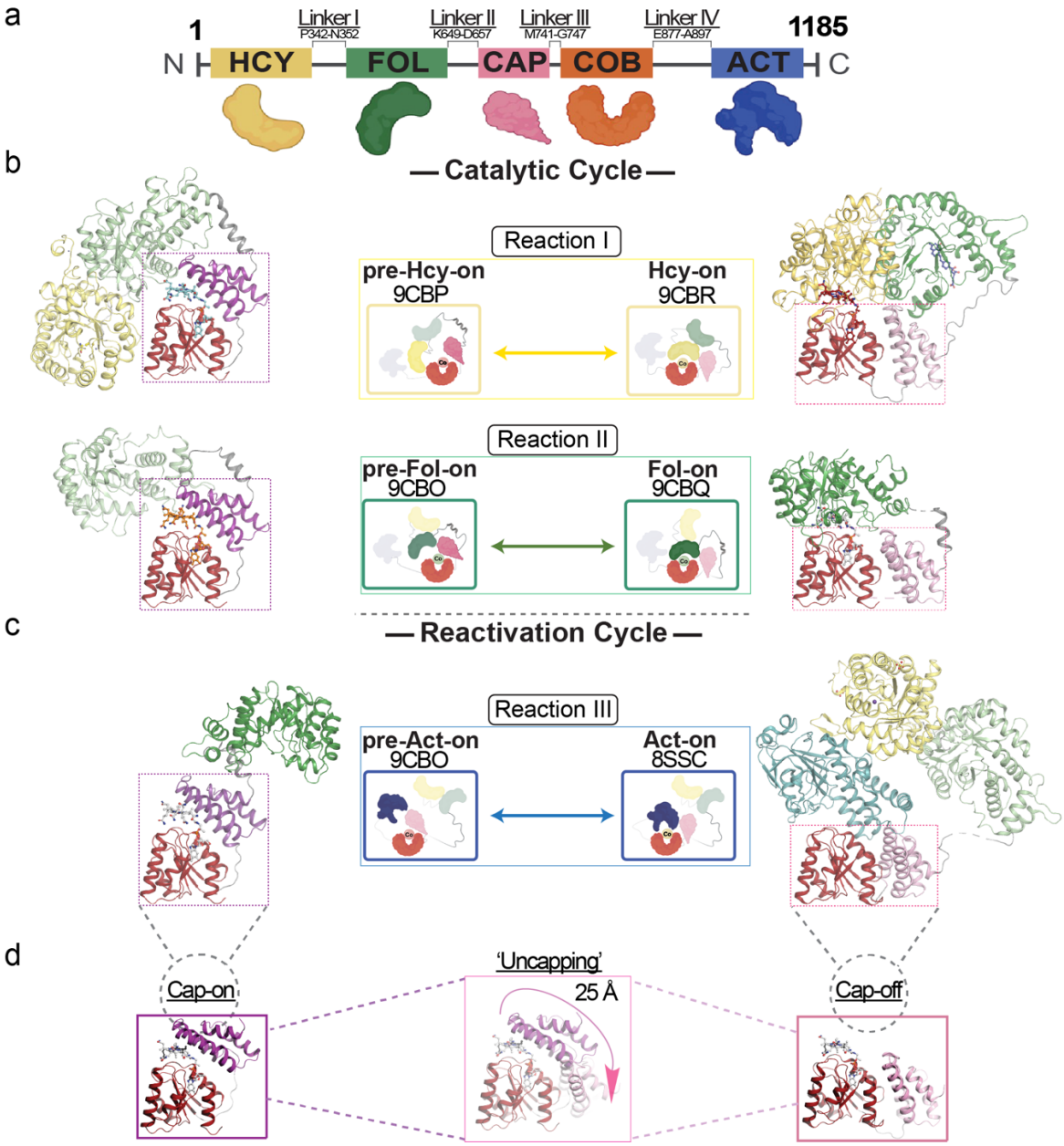

Figure 2. Methionine synthase conformational ensemble dictates chemical outcome. a Four compact substrate/cofactor binding (Hcy, Fol, Cob, and Act) and cofactor capping (Cap) domains are color-coded, with linkers displayed. **b** Experimentally determined Cap-On structures enable MS 'resetting', while Cap-Off structures facilitate ternary complex formation between the Cob and substrate binding domains as part of the catalytic cycle. **c** Similarly, Cap-on to Cap-off transitions enable chemistry as a part of the reactivation cycle. **d** The Cap-on states protect the cobalamin cofactor, and the uncapping transition results in a ~25 Å displacement of the Cap domain to a predetermined position nestled to the side of the Cob domain, allowing for domain access and chemistry by enabling access to the cobalamin cofactor.

Pre-Catalytic conformations expand Methionine Synthase's Conformational Ensemble

The ability to purify MS constructs that were previously unattainable provided an avenue for the ability to rationally sample and strategically limit the structural space MS could adopt via tactical truncations. By using the Fol:Cap:Cob tridomain construct, we envisioned capturing the ternary

catalytic folate demethylation complex (Fol-on). Similarly, we employed the Hcy:Fol:Cap:Cob tetradomain construct in an attempt to capture the ternary catalytic homocysteine methylation complex (Hcy-on).

Accordingly, *t*MS^{FolCapCob} was crystallized bound to its native cofactor, methylcobalamin (MeCbl), and its structure was solved to 3.34 Å (Figs. 2 and 3a, Supplementary Fig. 2, and Supplementary Table 1, 9CBO); using propylcobalamin (prCbl), we were able to crystallize *t*MS^{HcyFolCapCob}, solving the structure to 2.45 Å (Figs. 2 and 4a, and Supplementary Table 1, 9CBP). The latter reveals a Cap-on conformation (pre-catalytic, Supplementary Fig. 2, 9CBP), while the former captured two novel Cap-on conformations in one crystal, distinct from the only other reported Cap-on conformation of a muti-domain MS (Hcy:Fol:Cap:Cob, 8G3H)[11], where the folate binding site is pre-positioned to interact with the Cob domain (pre-Fol-on, Supplementary Fig. 3, 9CBO). While a third novel Cap-on structure was captured in the same crystal as the termed pre-Fol-on structure, further work is underway to confirm our preliminary assignment as a pre-catalytic conformation (proposed pre-Act-on, Supplementary Fig. 3, 9CBO).

Capturing three Cap-on conformations, two of which are distinct/unique (pre-Fol-on, pre-Act-on, Supplementary Fig. 2) and one that recapitulates 8G3H (pre-Hcy-on, Supplementary Fig. 2), indicates that the premise that 8G3H represents a “resting” state is an oversimplification and deficient/incomplete assignment of the overall and inherently complex mechanism that allows MS to interconvert between catalytically capable/relevant/competent conformations. Indeed, the three observed Cap-on states likely represent pre-catalytic intermediates that act as essential steps leading up to the three different methylations. While incapable of chemistry themselves, these reported Cap-on states act as gateways, allowing access to the three ternary conformations required for chemistry/catalysis to occur. While the authors termed their structure as *the* “resting” state, we argue that it represents one of at least three pre-catalytic/'resting' conformations. The capture of three distinct Cap-on states was wholly unexpected and indicates that the structural space MS samples prior to catalysis is more complex than previously thought.

The defining feature of the Cap-on conformations is the structured Fol:Cap linker (Linker II), which was found as an unstructured loop in the full-length *t*MS structure (8SSC)[9]. In the three pre-catalytic states presented here (Supplementary Fig. 2b) it is found as a structured and flexible helix. Even so, the structures reveal that the helix of Linker II is more structured in the pre-Hcy-on conformation and slightly less structured in the pre-Fol-on conformation, shortening the helix by 11.2 Å and shifting the N-terminal portion of the Fol:Cap linker 18.8 Å laterally (Supplementary Fig. 3). This partial melting of the helix in the pre-Fol-on allows Linker II to act as a hinge, as the domains themselves maintain their topology and move as rigid bodies (Supplementary Fig. 3). The hinge contracts and rotates the Fol domain 120° to orient the folate binding site toward and above the Cap:Cob domain, as opposed to its orientation in the pre-Hcy-on state, where the active site is facing away (Supplementary Fig. 3).

Consequently, these pre-catalytic structures demonstrate the importance of Linker II in allowing for proper and guided transitioning between Cap-on states. Indeed, conformational morphing indicates that each state can interchange freely via a lasso-like movement of Linker II (Supplementary Movie 1). This enables MS to 'reset' and cycle between pre-catalytic, Cap-on gateway conformations which can then transition to catalytic ones. As such, the status of Linker II is essential to transition between Cap-on states.

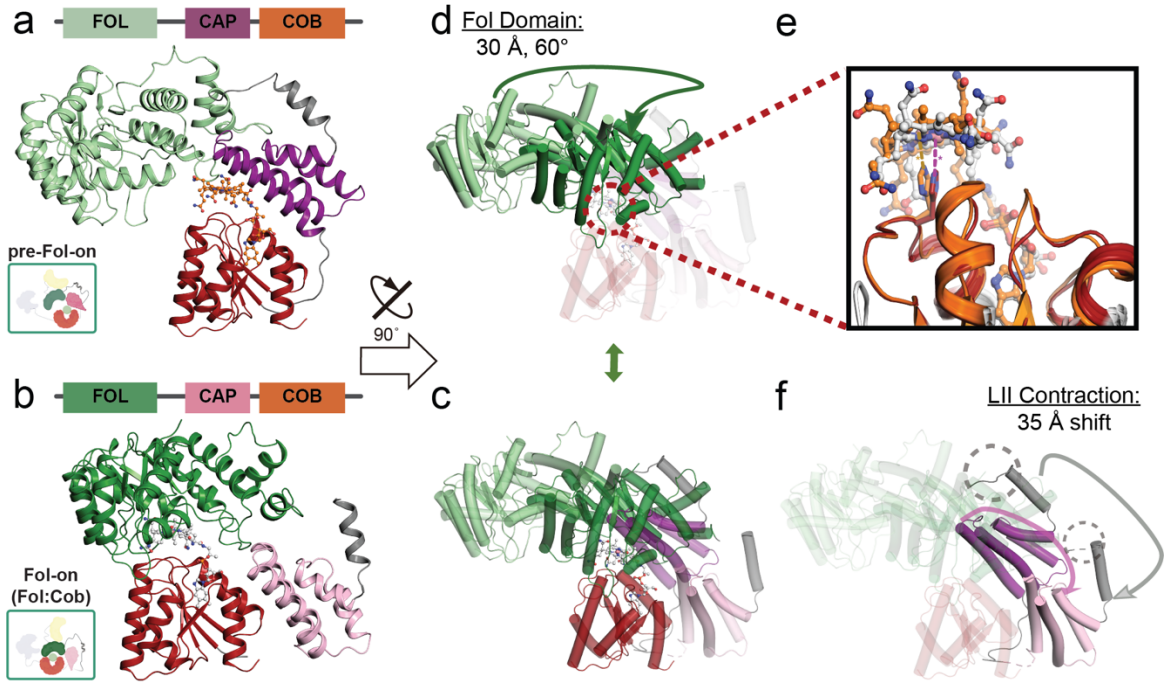

Figure 3. Structural comparison of pre-catalytic states and catalytic states (pre-Folate-on and Folate-on). a Structure of *t*MS^{FolCapCob} captured in the pre-Fol-on conformation colored by domain (Fol domain, pale-green; Cap, dark purple; Cob, orange) with the Fol:Cap linker shown in grey. **b** Structure of *t*MS^{FolCapCob} captured in a catalytic conformation (Fol, forest green; Cob, dark red; Cap, light pink) with the Fol:Cap linker shown in grey. Superposition of those structures are illustrated in **c**. The Cob domain was used as the reference for the structure alignment. The cobalamin cofactor must traverse 25 Å to form the Fol-on ternary complex. **d** Superposition using the Cob domain as a reference of the Fol domain *t*MS^{FolCapCob} structures using the same coloring scheme as **a** and **b**. Contraction of the Fol:Cap linker causes a 60° rotation coupled with a 30 Å translation of the Fol domain, while simultaneously uncapping the cobalamin cofactor bound in the Cob domain (**f**). **e** His761 distance between pre-catalytic and catalytic states in *t*MS^{FolCapCob}. The interactions between His761-Nε2 and the Co center are shown in dark orange (2.6 Å) and magenta (3.4 Å) dotted lines for pre-Fol-on and Fol-on, respectively.

Visualizing methyl-transfer in *t*MS

Folate demethylation (Fol-on) conformation

The use of truncated constructs with methylcobalamin and even propylcobalamin was not enough to yield the Cap-off states. The inability of propylcobalamin to yield a Cap-off state was particularly surprising, given that there is literature precedence for its use in preferentially binding cobalamin in a His-off, Cap-off state; these studies demonstrated that MS loaded with

propylcobalamin was trapped in the reactivation conformation (Act-on) and was found to be catalytically inactive[12,13]. This is especially surprising when considering that it was coupled with a tetradomain construct (*t*MS^{HcyFolCapCob}) lacking the Act domain, removing its ability to sample said reactivation conformation. For this reason, we next sought to exploit the robustness of our tMS model to protein engineering by introducing mutations designed to steer the conformational ensemble away from the His-on, Cap-on state and explored the use of bulkier, non-alkyl upper axial ligands that would further destabilize the Cap-on conformation(s) [8,14,15,16,17]. To that end, we selected γ-carboxypropyl cobalamin (cpCbl) (Fig. 1b), a synthetic cobalamin that does not support catalysis; using this analog, we were able to crystallize *t*MS$^{FolCapCob•D762G}$, solving the structure to 2.87 Å (Figs. 2b, 3b, and Supplementary Table 1, 9CBQ).

In the captured conformation (Fol-on), the Fol-domain is positioned over the Cob-domain, placing the MTF-binding site directly above cobalamin cofactor (Fig. 3b). The cofactor is bound in the His-on state, where His761 is coordinated through its imidazole side chain 3.4 Å from Co (Fig. 3e). The Cap domain, destabilized from its protective position, is displaced ~25 Å from the Cap-on state conformations[10,11] in a manner virtually identical in form and position to previously captured Cap-off structures, lying to the periphery of the Cob domain (8SSC, 8SSD, 8SSE, Supplementary Fig. 4)[9]. This suggests that the position of the displaced Cap domain is programmed, rather than random. The dramatic rearrangement of the cobalamin cofactor and its associated domain (Cob), transversing 25 Å after uncapping (Supplementary Fig. 3), is mediated by the structuring of Linker II in lieu of intradomain interactions, validating our previously proposed hypothesis that the flexibility of the linkers not observed in our previous structures must be key in orchestrating these domain movements[9].

The Fol:Cap linker, previously found as an unstructured loop in the full-length apo structure (8SSC)[9], is now found as a partially structured helix, denoting/demonstrating that the Fol:Cap linker contributes to the complexity and versatility of the MS structural ensemble. Starting from a Cap-on state (pre-Fol-on), this hinge must undergo a loop-helix transition to form the Fol-on ternary catalytic complex. In this case, the N-terminal portion of the linker is disordered (4 residues unmodeled); again, this small change results in a corresponding 34.5 Å shift of the linker and 60° rotation of the Fol domain (Fig. 3d and f, Supplementary Fig. 3). Combined with the Cap-off transition, this allows for the cobalamin cofactor to be completely buried by the new Fol:Cob intradomain interface/surface (Supplementary Fig. 4). The pre-catalytic to catalytic transition also results in repositioning of the cobalamin cofactor: the Co center is shifted ~1.5 Å laterally with an associated downward tilt of ~3°. The corrin ring, which experiences significant distortion, is more planar in the captured Fol-on state (Supplementary Fig. 5), due to an increase in the ligating His761 distance (2.2-2.6 Å from the Co center in pre-Fol-on versus 3.1 Å in the Fol-on state), relieving downwards “doming” towards the ligating His.In total, this structure represents the Fol-on (Fol:Cob) state, adopted for the methyl transfer from MTF to Cob(I). As the only/first catalytic structure visualized for any corrinoid folate enzyme, this structure gives

unique insight into the required orientation of the Fol and Cob domains and informs on how the initial methyl transfer to form methylcobalamin can proceed.

Previous structures of MTF-bound Corrinoid iron-sulfur protein/Methyltransferase (CFeSp/MeTr) were captured in an *en route* conformation, as the distance between the cofactor and MTF was too large to support catalysis (~8 Å) and further motions are required to bring the Co center closer to the methyl group[18]. SN_2 nucleophilic displacement, favored as the mechanism of methyl transfer in cobalamin-dependent methyltransferases[19,20], requires an expected reaction distance of 3-4 Å between the cobalt center and the MTF-methyl group. To determine if the orientation captured in the Fol-on structure could support catalysis, we modeled MTF into the active site found that the N5-methyl of MTF is positioned directly above and in-line with the cofactor, ~3.2 Å from Co-center (Supplementary Fig. 5, 6)[21]. Both the arrangement and proximity of the reacting centers indicate the captured state represents a catalytically competent structure, or a 'right-after-catalysis' state.

Encouraged by the ability to capture transient conformations using crystallography, we next sought to structurally interrogate the homocysteine methyltransfer reaction (Reaction II, Fig. 1).

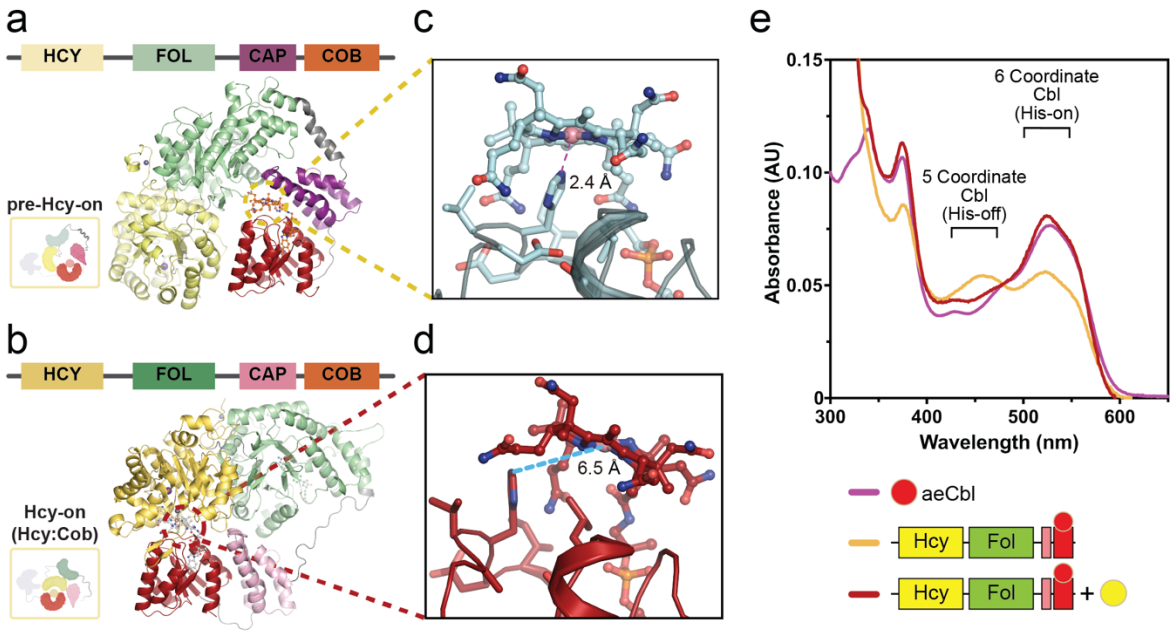

Figure 4. Structural comparison of pre-catalytic states and catalytic states (pre-Homocysteine-on and Homocysteine-on). a Structure of *t*MS^{HcyFolCapCob} captured in in the pre-Fol-on conformation colored by domain (Hcy domain, pale yellow; Fol domain, pale-green; Cap, dark purple; Cob, orange) with the Fol:Cap linker shown in grey. **b** Structure of *t*MS^{HcyFolCapCob} captured in a catalytic conformation (Hcy, yellow orange, Fol, forest green; Cob, dark red; Cap, light pink) with the Fol:Cap linker shown in grey. Superposition of those structures are illustrated in **c**. The Cob domain was used as the reference for the structure alignment. **d** His761 distance between pre-catalytic (light cyan, pre-Hcy-on) and catalytic states in *t*MS^{HcyFolCapCob} (brick red, Hcy-on). The cobalamin cofactor is displaced 3.8 Å laterally and is bound His-off in the catalytic conformation. **e** Free aminoethylcobalamin (aeCbl) shows a peak at approximately 530 nm, characteristic

of six-coordinate alkyl-cobalamin (magenta). Upon binding to *t*MS, the aeCbl spectrum exhibits an additional peak at around 460 nm, suggesting that a fraction of aeCbl binds in the His-off mode (five-coordinate) (golden yellow). Furthermore, the addition of excess exogenous homocysteine to the sample (tMS$^{HcyFolCob\ mut}$•aeCbl) induces changes in the spectrum (brick red). Given that cobalamin in the Cap-on state is known to adopt the six-coordinate state, it is proposed that cobalamin in the Hcy-on conformation adopts five-coordinate state.

Homocysteine methylation (Hcy-on) conformation

Having capitalized on the tridentate approach of rational non-native cofactor, truncated construct, and protein engineering use to capture transient conformations via crystallography, we next sought to capture the homocysteine methylation conformation (Hcy-on). Given that *t*MS^{HcyFolCapCob} was used, the sample space was inherently more expansive than that of the tridomain construct used to capture the Fol-on conformation. Consequently, the biochemical features associated with the Hcy-on conformation were explored via the use of non-native cobalamins and mutations designed to disfavor the Cap-on state captured (pre-Hcy-on) and favor the Cap-off state. The three Cap-on, pre-catalytic structures, namely the pre-Fol-on and pre-Hcy-on states, provided molecular level insights into the structural features that could gate entry to the Hcy-on state, particularly the role the Fol domain and Linker II play in structural transitions. The helical nature of Linker II in the pre-Hcy-on state, along with the helix-loop transition associated with the pre-to-Fol-on transition, provided the tantalizing prospect that capitalizing on/exploiting the flexibility of the linker by its partial melting could preferentially steer the ensemble towards catalytic states.

As such, the nature of the non-native cobalamin coordination bound to several *t*MS^{HcyFolCapCob} constructs was studied via UV-Vis spectroscopy, confirming that the constructs adopt both His-on and His-off binding modes (Fig. 4e). Addition of homocysteine shifts this equilibrium to the His-off state, despite using non-reactive cobalamins, with aminoethylcobalamin (aeCbl) having the most pronounced effects, yielding a visible color change from red/pink (His-on, 6 coordinate, Co(III)) to yellow (His-off, 5 coordinate, Co(III)) (Supplementary Fig. 7). The absence of the Act domain precluded sampling of the reactivation state, and the intriguing change to a yellow color, normally associated with cob(II)alamin (and thus inactivation), implied another set of states were being sampled in solution.

In light of these findings, mutations designed to disrupt the helical nature of the Fol:Cap linker and favor His-off cobalamin binding were introduced (Supplementary Fig. 8), with aeCbl used as the non-reactive cobalamin of choice. Using this mutated *t*MS construct and alternate cofactor coupling, we were able to crystallize *t*MS^{HcyFolCapCob}, solving the structure to 2.38 Å (Fig. 4 and Supplementary Table 1).

In the Hcy-on conformation, the Hcy-domain is positioned over the Cob-domain, placing the HCY-binding site directly above the cobalamin cofactor (Fig. 4b). The cobalamin cofactor is bound in the His-off state, where His761 is ~6.3 Å from Co (Fig. 4d). Indeed, crystals were

found to be yellow in color, as compared to the red/pink color observed for the pre-Hcy-on crystal (Supplementary Fig. 7). Akin to the Fol-on structure, there is a dramatic rearrangement of the cobalamin cofactor and its associated domain Cob, transversing ~45 Å after uncapping (Fig. 5, Supplementary Fig. 3). The Fol:Cap linker is found to undergo a helix-loop transition, confirming its role in facilitating transitions within the catalytic ensemble (Fig. 5).

The cobalamin cofactor in the catalytic structure is laterally shifted ~3.8 Å relative to its pre-catalytic state with a concurrent ~20° tilt, culminating in a change from a distorted to more planar corrin ring (Supplementary Figs. 9, 10). The corresponding changes associated with the cobalamin cofactor are analogous to those observed in previous MS structures in the reactivation conformation (Act-on), particularly the His-on versus His-off states/transition[6,9,22,23]. In total, these structures represent the Hcy-on (Hcy:Cob) state, which is adopted for the methyl transfer from methylcobalamin to homocysteine to yield methionine and Cob(I) (Reaction II, Fig. 1a).

Homocysteine methylation/methionine formation has been postulated to occur via an SN_2 mechanism whereby Zn acts as a Lewis acid to prime homocysteine for nucleophilic abstraction of the methyl group from methylcobalamin[19,24,25]. To determine if the orientation captured in the Hcy-on structures could support catalysis, we modeled HCY into the active site using the Hcy domain of our pre-Hcy-on structure and found that the sulfur moiety of HCY is positioned directly above and in-line with the cofactor, ~4.4 Å from Co (Supplementary Fig. 10). Modeling methylcobalamin in the active site shows that the distance between the sulfur/thiolate moiety and the methyl group of methylcobalamin is ~2.1 Å. As such, this structure represents one that is catalytically competent for HCY methylation, indicating that the combination of non-native cofactors and rational protein engineering allowed for the crystallographic snapshot of a transient complex.

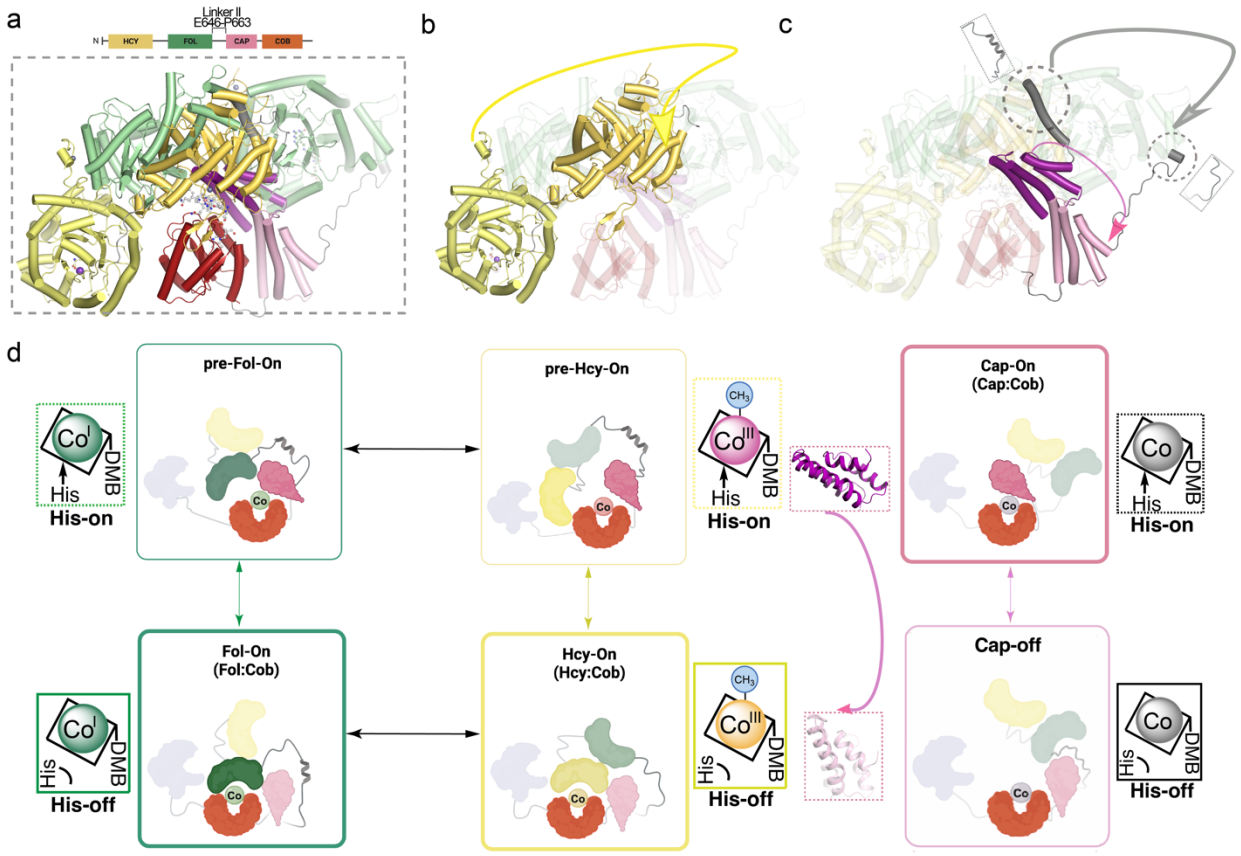

Figure 5. Large domain motion and linker reorganization define pre-catalytic and catalytic (pre-Homocysteine-on and Homocysteine-on) transitions. a Superposition of the Hcy and Fol domains using the Cob domain as a reference. *t*MS^{HcyFolCapCob} structures are shown as cartoons use the same coloring scheme as in Figure 3. **b** Contraction of the Fol:Cap linker causes a dramatic 40 Å repositioning of the Cob domain with the Hcy domain to form the Hcy-on ternary complex. **c** The Fol:Cap linker undergoes a helix-loop transition. The near complete melting of the helix enables the Hcy:Fol domains to move as rigid bodies after uncapping, repositioning the Hcy binding site and domain directly above the Cob domain and its bound cobalamin cofactor. **d** A revised cartoon model representing the transitions between Cap-on (pre-catalytic) and Cap-off (ternary, catalytic states). In all Cap-on structures, cobalamin is bound His-on. The Cap domain is placed in an identical position in all Cap-off structures, guided by Linker III, while Linker II helix-loop transitions mediate HcyFol domain motions.

The Fol domain is required for Homocysteine Methylation

To interrogate the biochemical basis of the role of the Fol domain, particularly in the homocysteine methyltransferase reaction, we employed a UV-Vis assay using the Hcy, Hcy:Fol, and Cap:Cob domains in trans[26]. The excised domains were chosen to provide a simpler, minimal model sufficient to study the ability of MS to perform homocysteine methylation[27]. Methylcobalamin consumption was monitored using UV-Vis to quantify the activity of various kinds of *t*MS domains (Fig. 6). The Hcy:Fol didomain and the isolated Hcy domain of tMS (designated *t*MS^{HcyFol} and *t*MS^{Hcy}, respectively) contain the homocysteine-binding sites.

Methylcobalamin was prepared and used in its free form and complexed with the Cap:Cob didomain (*t*MS^{CapCob}).

Consumption of exogenous methylcobalamin was detected in the presence of both *t*MS ^{HcyFol} and *t*MS^{Hcy} (Fig. 6) but not in their absence (Supplementary Fig. 11). The consumption of methylcobalamin bound to *t*MS^{CapCob} was observed with *t*MS^{HcyFol} (Fig. 6c) but not with *t*MS^{Hcy} (Fig. 6d). These data suggest that the Fol domain is important for the formation of the Hcy-on conformation, and without it, a catalytically competent Hcy-on ternary complex cannot be formed[7,8,11 ,28].

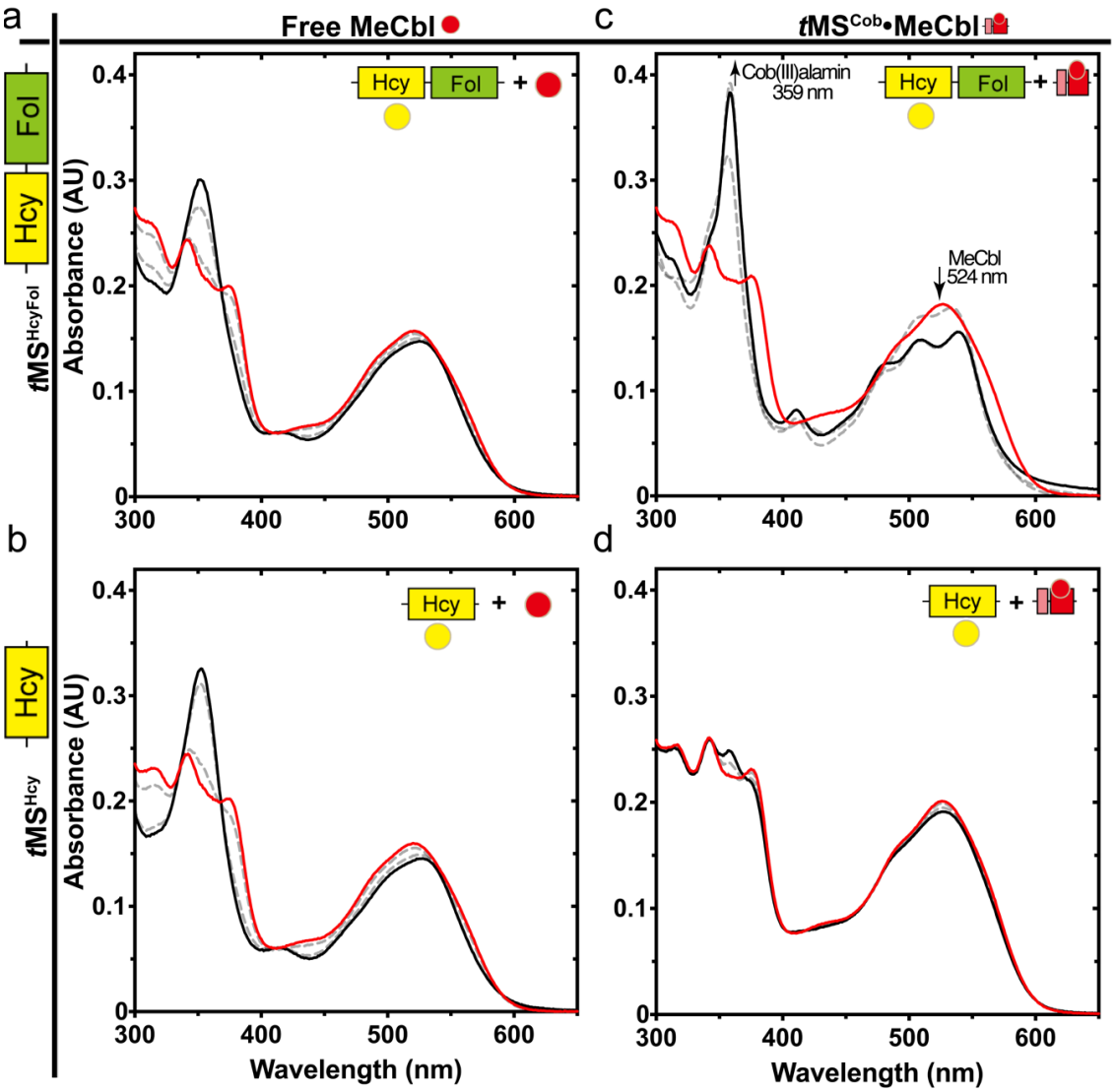

Figure 6. **Homocysteine methylation occurs in the His-off state and requires the Fol domain.** **a** Effects of *t*MS domain fragments on methylcobalamin:homocysteine methyltransferase reaction. The time-dependent spectral changes of methylcobalamin (MeCbl) in the presence of homocysteine were monitored at 50 ˚C for up to 10 minutes after adding homocysteine (final concentration of 100 μM) using 20 μM of free (non-protein bound) MeCbl incubated in the presence of 2 μM *t*MS constructs (**a** and **b**) or MeCbl (23 μM) was bound to the isolated *t*MS^{CapCob} domains first (**c** and

d). Red lines represent the initial time point, with black lines representing the end point (final 10 min); gray lines represent intermediary timepoints (2, 5 min). Note that the the presence of the Fol domain is required for activity when methylcobalamin is protein bound (**c**). Free homocysteine and methylcobalamin did not react (Supplementary Fig. 11), similar to *t*MS bound cobalamin (**d**). Free cobalamin can react minimally with *t*MS bound homocysteine, presumably due to the lack of the Cap domain and the ability of the Hcy domain to activate homocysteine.

Proposed mechanism for MS catalysis

The Fol domain governs access to catalytic conformations

Our previously captured *t*MS structures (8SSC, 8SSD, and 8SSE) highlighted the preformed cobalamin pocket, which is solvent-exposed and thus readily accessible even *in crystallo*[9]. Similarly, previous structures of MS excised domains revealed that the Hcy and Fol domains were preformed, with minimal microenvironment changes in the substrate binding pocket induced upon ligand/substrate binding[21,29,30]. Even so, enzymes that bind multiple substrates, particularly those that follow a ping-pong mechanism (in the case of MS, two ping-pong mechanisms)[28], must exert global control over the conformational rearrangements that would allow access to the cobalamin cofactor (i.e. the formation of a ternary complex with the Cob domain and a substrate domain).

The first catalytic step in the MS catalytic cycle is the demethylation of MTF using Co(I) to form methylcob(III)alamin and THF; intriguingly, while purification of *t*MS routinely results in copurification with MTF, the use of the *t*MS^{FolCapCob} tridomain did not yield the MTF-bound structure. However, the *t*MS^{HcyFolCapCob} tetradomain does copurify with MTF. Given that the second catalytic step in the catalytic cycle is the methylation of HCY using methylcob(III)alamin to form methionine and Co(I), MS that lacks MTF could undergo futile cycling, with the generated Co(I) cofactor being prone to oxidative inactivation. As such, the importance of MTF-binding, and thus of the Fol domain, makes intuitive sense. Even so, the finding that only *t*MS^{HcyFol} was active in the trans assay using methylcobalamin loaded *t*MS$^{Cap:Cob}$ indicates that the Fol domain plays a critical role in guiding the conformation rearrangement necessary for the formation of the Hcy-on ternary complex (Fig. 6), likely through its role in destabilizing the Cap-on state (uncapping activity)[11]. Whether the Hcy domain itself is necessary for proper MTF-binding and reactivity remains unexplored/unknown. Additionally, the flexible linker region connecting Fol:Cap (Linker II) must be taken into consideration, as the presented structures indicate that while the linker is flexible, it can become ordered, forming a structured helix that can, putatively, act as a “swiveling point”/hinge. This coil-helix transition would represent a tantalizing explanation for why the Fol domain is necessary for the formation of the Hcy-on conformation and would provide a guided mechanism by which MS telegraphs/integrates substrate-binding information with cofactor status to undergo the pre-requisite rearrangements necessary for catalysis[7,8,11,28].

Linker regions guide domain rearrangements centered on the cobalamin Cofactor (Cob Domain)

Our previous structures of *t*MS (8SSC, 8SSD, 8SSE) were all found in the reactivation state (Cap-off, Act-on). The Fol-on structure provides the first insight that interdomain linkers, in this case the Fol:Cap linker (Linker II), play an important role in facilitating the formation of specific conformations, undergoing a loop-helix transition. The Hcy-on structures likewise use this Fol:Cap linker, with the transition between the Fol-on to the Hcy-on states restoring the helical nature of the region (hinge); however, the captured pre-catalytic conformations, so called pre-Fol-on and pre-Hcy-on, also result in transitions between the loop and helical state, where the pre-Hcy-on state adopts a fully structured Linker II state (Supplementary Figs. 2, 3, and 9). The Hcy:Fol linker, being rigid, is not found to change significantly[29]. As such, the Fol:Cap linker seems to play an outsized role in dictating and influencing the formation of catalytically-competent ternary complexes in the MS catalytic cycle, along with intermediates contained therein.

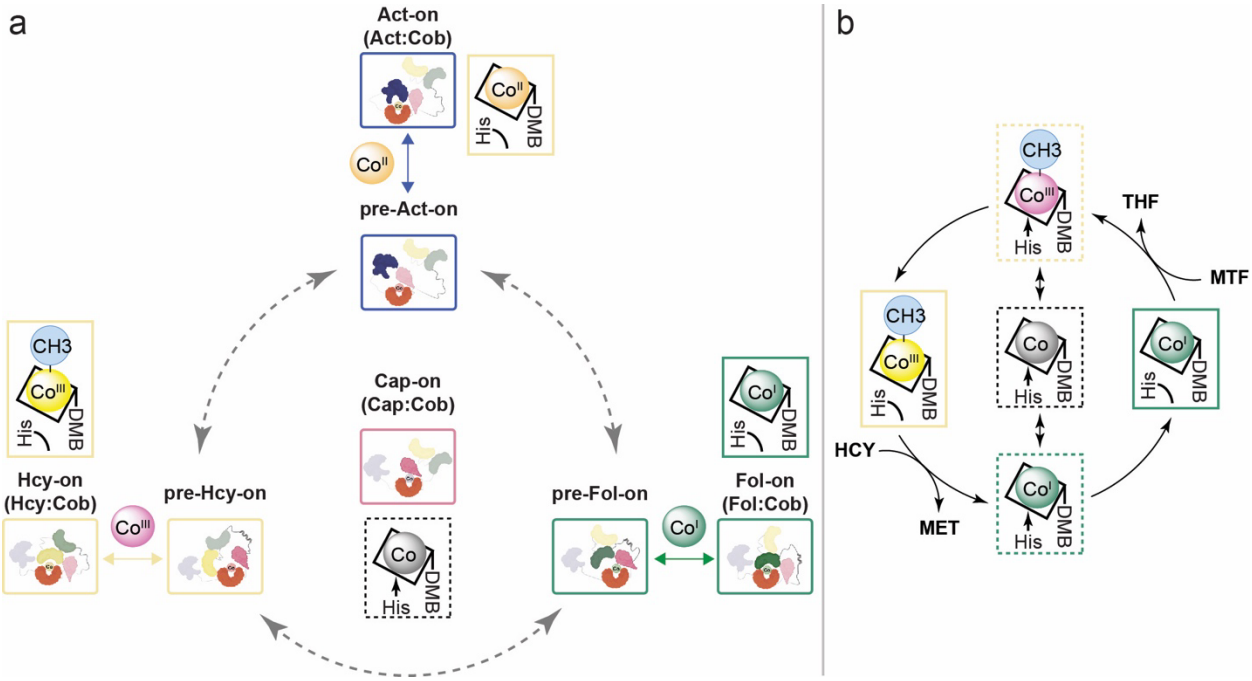

Figure 7. Conformational transitions during catalysis are mediated by the Hcy:Fol linker and signaled by His761.

Alignment of the catalytic structures, including the previously obtained Act-on reactivation structures, indicate that the Cap-off Cob domain remains static, with the substrate-binding domains undergoing drastic rearrangements in order to orient themselves above the Cob domain to form a ternary complex (Supplementary Figs. 2, 3, and 4). As such, the structural rearrangements observed center on the Cap:Cob domains, with substrate-binding domains vying for access to the protected (Cap-on) Cob domain. The finding that the Hcy:Fol domain is necessary for formation of the Hcy-on state indicates that the Fol domain plays a key role in guiding the conformational ensemble, even if it lacks the Fol:Cap linker. In this case, the Cap:Cob linker (Linker III) could play a role in mediating the uncapping motion required for cobalamin access, placing the Cap domain in a predetermined position. Morphing of pre-

catalytic (Cap-on states, pre-Fol-on, pre-Hcy-on) and catalytic (Cap-off, Fol-on, Hcy-on) structures show that the Fol:Cap linker acts as a swiveling point (hinge) around which the Hcy:Fol domains, presumably, use the Fol domain to initiate "uncapping" of the Cob domain (Supplementary Movies 2 and 3). Even in the Cap-on structures, the Cap:Cob domain remains relatively static (Supplementary Figs. 2 and 15). It seems that the Fol domain, in conjunction with the Fol:Cap linker, plays a critical role in initiating and thereafter guiding the conformational ensemble during catalysis, while the Cap:Cob linker allows for proper repositioning of the Cap domain in one of two states (Cap-on or Cap-off).

Discussion

Given that MS can adopt numerous conformations in solution, exactly how MS regulates these domain arrangements remains an open question in the field[5,6,7,8]. In this work, we have leveraged our previously discovered thermophilic methionine synthase homolog (*t*MS)[9] to structurally interrogate the conformations behind MS catalysis. The conformational ensemble of MS has been expanded, including pre-catalytic states that serve to gate entry to the catalytic cycle. The first catalytic structures of MS, poised for MTF demethylation (Fol-on) and for HCY methylation (Hcy-on) have been captured, adding previously unattainable insights into the residues and global rearrangements that dictate catalytic activity. In addition, this work sheds light on outstanding questions that have been the subject of research for decades, and the insights gleaned herein will serve to expand our understanding of MS and explore MS as a biocatalytic tool.

Our biochemical and structural data indicate that five coordinate His-off methylcob(III)alamin is formed during catalysis (Figs. 4, and 5, Supplementary Figs. 7, 9, and 10). Our Hcy-on structure captures this five-coordinate Co(III) state. While the Fol-on complex is six-coordinate (His-on, Co(III)), we posit that this represents a 'right-after-catalysis' state, given that the His-on bound cpCbl is in the Co(III) state and thus mimics methylcob(III)alamin (Supplementary Fig. 5). Further work is needed to demonstrate the presence of the same five coordinate His-off cobalamin (methylcob(III)alamin/Co(III)) species in folate demethylation (right after catalysis) though its observation in the Hcy-on state lends credence to its predicted role; similarly, we posit that the required transition from five coordinate methylcob(III)alamin/Co(III) to four coordinate Co(I) after homocysteine methylation necessitates a state where said species is found His-on (Co(I)), presumably right after catalysis.

Captured structures of cobalamin-dependent methyltransferases and biochemical studies have demonstrated that His-on ligation is not necessary for methyl abstraction and indeed might instead stabilize methylcobalamin, given the observation that methylcobinamide (MeCbi, pentacoordinate) is more reactive towards demethylations[18,20,31,32,33,34,35,36,37]. Consequently, we propose that His-ligated hexacoordinate methylcob(III)alamin is found prior to catalysis, stabilized and protected in a resting, Cap-on state. Subsequent "uncapping" triggers His-off binding to form pentacoordinate methylcob(III)alamin, the active methyl transfer agent, which

forms tetracoordinate cob(I)alamin after catalysis as its byproduct. Thereafter, the supernucleophilic tetracoordinate cob(I)alamin can be stabilized/sequestered via His ligation to form pentacoordinate cob(I)alamin, triggering "recapping" to protect the cofactor (Fig. 7, Supplementary Fig. 12).

Overall, this revised mechanistic and structural model synthesizes the wealth of biochemical data with unprecedented molecular level structural insights, providing a new unified framework with which to understand cobalamin-dependent methyltranferases such as methionine synthase (Fig. 7, Supplementary Fig. 12). Starting from one of three Cap-on, His-on states (Fig. 6), MS can alternate between these three pre-catalytic conformations through rigid body motion of the Hcy:Fol domain towards the Cob domain (pre-Fol-on, pre-Hcy-on) or away from it (pre-Act-on), all mediated by the remarkable polymorphism of Linker II. Linker II is a versatile element capable of adopting three distinct structural conformations. This flexibility enables it to rearrange and reposition the domains attached to its termini. His-off ligation of cobalamin acts as a switch to allow for gated entry from pre-catalytic to catalytic transitions and vice-versa (Fig. 7). Structural transitions to catalytic states are signaled/gated by His ligation, mediated by the Fol:Cap hinge (Linker II), programmed rigid body movement of the Cap:Cob domain via the Cap:Cob linker (Linker III), and substrate domain association to form a ternary complex ready for catalysis. In this manner, MS harnesses the catalytic potential of cobalamin while avoiding futile cycling, leveraging unheralded structural motifs to orchestrate the dramatic rearrangements required to perform three improbable chemistries.

Methods

Cobalamin Analogue Synthesis

Cyanocobalamin (CNCbl) was purchased from Sigma/MilliporeSigma. cobalamin analogues were synthesized following previously established methods[38,39,40]. Briefly, CNCbl reduced by $NaBH_4$ was mixed with 4-chlorobutyric acid (Sigma/MilliporeSigma), 2-chloroethylamine hydrochloride (Sigma/MilliporeSigma), or n-propyl iodide (Sigma/MilliporeSigma) to yield γ-carboxypropyl-cobalamin (cpCbl), aminoethyl-cobalamin (aeCbl), and propyl-cobalamin (prCbl), respectively.

Construction of *t*MS Expression Vectors

Expression vectors for truncated *t*MS expression were generated using the ligation-independent cloning (LIC). Molecular cloning was conducted using pMCSG7 as the expression plasmid DNA vector and *E. coli* XL1-Blue as the host cell. DNA amplification was performed using Pfu Turbo Cx DNA polymerase (Agilent) and the MJ Research Thermal Cycler. DNA sequencing was accomplished with The BigDye Terminator v3.1 cycle sequencing kit and the ABI 3500 DNA sequencer from Applied Biosystems. All constructed bacterial expression vectors were designed to produce truncated *t*MS with a hexa-histidine tag and a Tobacco Etch Virus (TEV) protease cleavable sequence at the N-terminus.

The genes encoding truncated *t*MS were amplified by PCR, using pET(*t*MS^{wt}) as the template, obtained from the Riken BioResource Center[41]. Subsequently, these amplicons were integrated into a pMCSG7 vector using the ligation-independent cloning technique to generate truncated *t*MS expression vectors. To express tridomain *t*MS, pMCSG7(*t*MS^{FolCob}) was constructed, encompassing the Fol, Cap, and Cob domains; pMCSG7(*t*MS^{HcyFolCob}) was prepared in a similar fashion to express tetradomain *t*MS, containing all domains except for the Act domain. Didomain and single domain vectors to express the constructs used for assays were similarly generated, designated pMCSG7(*t*MS^{CapCob}), pMCSG7(*t*MS^{HcyFol}), and pMCSG7(*t*MS$^{\Delta N35Hcy}$). Mutant constructs were made by site-directed mutagenesis (QuikChange, Agilent). Mutant constructs of the tetradomain *t*MS used for crystallography include several mutations: pMCSG7(*t*MS$^{HcyFolCob\ F110A,E123A,E124A,Y296A,D651A,P652A,G653A}$/*t*MS$^{HcyFolCob\ DPG2A\ dEE\ F110A,Y296A}$) used for crystallization of Pre-Hcy-on (mutant 1/construct 1) and pMCSG7(*t*MS$^{HcyFolCob\ F110A,E123A,E124A,R268A,N283G,D651A,P652A,G653A,D759A,N774H,R826A}$/*t*MS$^{HcyFolCob\ DPG2A\ dEE\ dRR\ F110A,N283G,D759A,N774H}$) used for crystallization of Hcy-on (mutant 2/construct 2), will be referred to as such in the methods for the sake of simplicity. A complete list of the bacterial strains, plasmids, and primers used in this study are listed in Supplementary Table 2.

Expression of *t*MS Constructs

E. coli BL21star(*DE3)* was transformed with the desired expression vectors for protein expression. *E. coli* transformed with the desired pMCSG7(*t*MS) constructs were propagated at 37 °C in Luria Broth containing 50 µg/mL ampicillin, and protein overexpression was induced using autoinduction media[42,43]. *E. coli BL21star(DE3)* transformed with pMCSG7(*t*MS$^{FolCob\ D759A}$) were propagated at 37 °C in Luria Broth containing 50 µg/mL ampicillin and protein overexpression was induced using Isopropyl β-D-1-thiogalactopyranoside (IPTG) (final concentration of 0.1 mM). In the case of *t*MS$^{HcyFolCob\ mut1}$, $ZnCl_2$ was added to the medium (0.5 mM) and protein overexpression was induced using autoinduction media. Cells were propagated at 30°C with shaking at 250 rpm overnight prior to harvesting via centrifugation and stored at −80 °C.

***t*MS Protein Purification**

Immobilized metal chelate affinity (IMAC) chromatography was employed to purify recombinant *t*MS (HisTrap Chelating HP, Cytvia, 5 mL), using a $NiSO_4$ charged column for all constructs except for *t*MS^{HcyFolCob}, where a $ZnSO_4$ charged column was used.

*t*MS$^{FolCob\ D759A\bullet MeCbl}$ (Pre-Fol-on)

For holoenzyme purification with Mecobalamin (*t*MS$^{FolCob\ D759A}$, *t*MS^{CapCob}), the harvested cell pellet was first resuspended in 50 mM potassium phosphate buffer (KPB) (pH 7.4), 0.3 M sodium chloride, (4–5 mL per 1 g of pellet), to which lysozyme (0.1 mg/mL) and PMSF (1 mM) were added. The resuspended cell pellet was lysed via sonication (4 °C, 5 s on, 5 s off, 5 min total). The crude lysate was centrifuged (15 min × 3, 10,000 × g, 4 °C) decanting the supernatant to remove any cellular debris/pellet. Methylcobalamin (MeCbl) (Millipore Sigma) was added to

the crude supernatant (20 mM) to form holo-*t*MS. The crude extract with Mecobalamin was incubated at 70 °C for 15 min, then centrifuged (15 min, 10,000 × g, 4 °C). The supernatant was pooled and filtered via vacuum (0.45 µm), to which imidazole was added (20 mM) and the supernatant was applied/loaded onto a Ni-affinity column (His-trap Chelating HP, Cytvia, 5 mL) equilibrated with 50 mM KPB, pH 7.4, and 20 mM imidazole. The column was washed with 50 mM KPB, pH 7.4, 0.3 M sodium chloride, 20 mM Imidazole (5 CV), then 50 mM imidazole (5 CV), and the protein was eluted in bulk with buffer consisting of 50 mM KPB, pH 7.4, 0.3 M sodium chloride, and 80 mM imidazole (8 CV) and 150 mM Imidazole (3 CV). Red-colored fractions were collected and subjected to a TEV digest, with dialysis at 4 °C overnight (50 mM KPB, pH 7.4). The dialyzed sample was incubated at 70 °C for 15 min to quench the TEV digest, then centrifuged (15 min, 10,000 × g, 4 °C). The resulting supernatant was filtered (vacuum, 0.45 µm) and concentrated via centrifugation in 50 mM KPB, pH 7.4 to yield purified *t*MS$^{\text{FolCob D759A•MeCbl}}$ (~10 mg/mL), which was stored at 4 °C or flash-frozen for long-term storage at 80 °C.

*t*MS$^{\text{CapCob•MeCbl}}$

*t*MS$^{\text{CapCob}}$ was prepared similarly, save for the use of a TEV digest. Following IMAC purification and pooling of red-colored fractions, the combined fractions were subject to dialysis at 4 °C overnight (50 mM KPB, pH 7.4). The dialyzed sample was concentrated via centrifugation in 50 mM KPB, pH 7.4 to yield purified *t*MS$^{\text{CapCob}}$ (~10 mg/mL), which was stored at 4 °C or flash-frozen for long-term storage at -80 °C.

*t*MS$^{\text{FolCob D762G•cpCbl}}$ (Fol-on)

Purification of *t*MS$^{\text{FolCob D762G}}$ was conducted similarly, with no added cobalamin. The harvested cell pellet was resuspended in 50 mM KPB (pH 7.4) (~5 mL/1 g of the pellet), to which lysozyme (0.1 mg/mL) and PMSF (0.1 mM) were added. The resuspended cell pellet was lysed via sonication (4 °C, 5 s on, 5 s off, 5 min total). The crude lysate was centrifuged (45 min, 20,000 × g, 4 °C) decanting the supernatant to remove any cellular debris/pellet. To the crude supernatant was added Imidazole (final concentration, 20 mM) before FPLC purification using a modified IMAC bulk elution (equilibration buffer: 50 mM KPB, pH 7.4, 20 mM Imidazole, wash buffer: 50 mM KPB, pH 7.4, 300 mM NaCl, 50 mM Imidazole, elution buffer A: 50 mM KPB, pH 7.4, 300 mM NaCl, 80 mM Imidazole, elution buffer B: 50 mM KPB, pH 7.4, 300 mM NaCl, 150 mM Imidazole) , with the desired protein eluting at 80 mM and 150 mM Imidazole. Fractions containing protein as confirmed by SDS–PAGE were then pooled, and an ammonium sulfate cut was used to remove any impurities, using an equal volume of saturated ammonium sulfate (~4 M) to achieve a final concentration of 50% (w/v). The mixture was centrifuged (10,000 × g, 10 min, 4 °C) to pellet any precipitated protein. The supernatant was carefully decanted to avoid disturbing the pellet; the pellet was resuspended in 0.1 M KPB, pH 7.4, 2 mM DTT (10 mL). A TEV digest and overnight dialysis (4 °C, 0.1 M KPB, pH 7.4, 2 mM DTT) followed. To the dialyzed sample containing ~135 µM apo-*t*MS$^{\text{FolCob D762G}}$ was added γ-carboxypropyl cobalamin (cpCbl,~170 µM) and the TEV digest quenched by heating at 60 °C

(15 min), then centrifuged (10 min, 4,000 × g, 4 °C). The resulting supernatant was loaded onto a pre-equilibrated desalting column (PD-10, GE/Cytvia, 50 mM KPB, pH 7.4) to remove excess cpCbl and concentrated via centrifugation in 50 mM KPB, pH 7.4 to yield purified holo-*t*MS$^{\text{FolCob D762G•cpCbl}}$ (~10 mg/mL), which was stored at 4 °C or flash-frozen for long-term storage at -80 °C.

Purification of apo constructs (*t*MS$^{\Delta N35Hcy}$, *t*MS^{HcyFol}) was conducted similarly, with no added cobalamin.

*t*MS$^{\Delta N35Hcy}$

The harvested cell pellet was resuspended in 50 mM Tris (pH 7.4), 0.1 M NaCl (~5 mL/1 g of the pellet), to which lysozyme (0.1 mg/mL) and PMSF (0.1 mM) were added. The resuspended cell pellet was lysed via sonication (4 °C, 5 s on, 5 s off, 5 min total). The crude lysate was centrifuged (10 min, 8,000 × g, 4 °C) decanting the supernatant to remove any cellular debris/pellet. The crude supernatant was subjected to a heat-treatment step at 60 °C (15 min), then centrifuged (10 min, 4,000 × g, 4 °C), decanting the supernatant to remove any cellular debris/pellet. To the crude supernatant was added Imidazole (final concentration, 50 mM) before FPLC purification using a modified IMAC bulk elution (equilibration buffer: 50 mM Tris, pH 7.4, 0.1 M NaCl, 50 mM Imidazole, wash buffer: 50 mM Tris, pH 7.4, 0.3 M NaCl, 50 mM Imidazole, elution buffer: 50 mM Tris, pH 7.4, 0.3 M NaCl, 200 mM Imidazole) , with the desired protein eluting at 200 mM Imidazole. Fractions containing protein as confirmed by SDS–PAGE were then pooled. The combined fractions were subject to dialysis at 4 °C overnight (50 mM Tris, pH 7.4), to which TCEP was added (final concentration, 1 mM), followed by a second heat-treatment step at 60 °C (15 min) then centrifuged (10 min, 4,000 × g, 4 °C). The resulting supernatant was concentrated via centrifugation in 50 mM Tris, pH 7.4, 1 mM TCEP to yield purified *t*MS$^{\Delta N35Hcy}$ (~10 mg/mL), which was stored at 4 °C or flash-frozen for long-term storage at -80 °C.

*t*MS^{HcyFol}

The harvested cell pellet was resuspended in 50 mM KPB (pH 7.4) (~5 mL/1 g of the pellet), to which lysozyme (0.1 mg/mL) and PMSF (0.1 mM) were added. The resuspended cell pellet was lysed via sonication (4 °C, 5 s on, 5 s off, 5 min total). The crude lysate was centrifuged (10 min, 8,000 × g, 4 °C) decanting the supernatant to remove any cellular debris/pellet. The crude supernatant was subjected to a heat-treatment step at 70 °C (15 min), then centrifuged (10 min, 4,000 × g, 4 °C), decanting the supernatant to remove any cellular debris/pellet. To the crude supernatant was added Imidazole (final concentration, 20 mM) before FPLC purification using a modified IMAC bulk elution (equilibration buffer: 50 mM KPB, pH 7.4, 50 mM Imidazole, wash buffer: 50 mM KPB, pH 7.4, 0.3 M NaCl, 50 mM Imidazole, elution buffer: 50 mM Tris, pH 7.4, 0.3 M NaCl, 80 mM Imidazole), with the desired protein eluting at 80 mM Imidazole. Fractions containing protein as confirmed by SDS–PAGE were then pooled. The combined fractions were

subject to dialysis at 4 °C overnight (50 mM KPB, pH 7.4). The resulting dialyzed sample was concentrated via centrifugation in 50 mM KPB, pH 7.4 to yield purified *t*MS^{HcyFol} (~10 mg/mL), which was stored at 4 °C or flash-frozen for long-term storage at -80 °C.

Purification of *t*MS^{HcyFolCob} constructs was conducted similarly, without added cobalamin, but using a $ZnSO_4$-loaded IMAC column (GE/Cytvia, 5 mL).

*t*MS$^{HcyFolCob\ mut1•prCbl}$(pre-Hcy-on)

The harvested cell pellet was first resuspended in 50 mM potassium phosphate buffer (KPB) (pH 7.4) (4–5 mL per 1 g of pellet), to which lysozyme (0.1 mg/mL) and PMSF (1 mM) were added. The resuspended cell pellet was lysed via sonication (4 °C, 5 s on, 5 s off, 5 min total). The crude lysate was centrifuged (45 min, 20,000 × g, 4 °C) decanting the supernatant to remove any cellular debris/pellet. The supernatant was pooled and filtered via vacuum (0.45 µm), to which imidazole was added (20 mM) and the supernatant was applied/loaded onto a Zn-affinity column (His-trap Chelating HP, Cytvia, 5 mL) equilibrated with 50 mM KPB, pH 7.4, and 20 mM imidazole. The column was washed with 50 mM KPB, pH 7.4, 0.3 M NaCl, 20 mM Imidazole (1 CV), then 50 mM imidazole (5 CV), and the protein was eluted in bulk with buffer consisting of 50 mM KPB, pH 7.4, 0.3 M sodium chloride, and 80 mM imidazole (10 CV) and 150 mM Imidazole (3 CV). Fractions containing protein as confirmed by SDS–PAGE were then pooled and subjected to a TEV digest, with dialysis at 4 °C overnight (50 mM KPB, pH 7.4). The dialyzed sample was incubated at 50 °C for 15 min to quench the TEV digest. Following clarification of the supernatant by centrifugation (10,000 × g, 10 min, 4 °C) and filtration (vacuum, 0.45 µm), the clarified supernatant was loaded onto a pre-equilibrated HiLoad 16/600 Superdex 200 pg column (Cytvia) (2 CV of SEC Buffer: 25 mM Tris, pH 7.4, 0.1 M KCl, 1 mM TCEP), yielding the desired protein (~95 kDa). The protein was found to elute as a monomer, with minimal to no aggregation visible. Fractions containing the desired protein, as judged by SDS–PAGE, were pooled and concentrated via centrifugation in 25 mM Tris, pH 7.4, 0.1 M KCl, 1 mM TCEP to yield purified apo-*t*MS$^{HcyFolCob\ mut1}$ (~15 mg/mL). To the purified apo protein (~150 µM) was added propylcobalamin (prCbl, ~170 µM). The resulting mixture was loaded onto a pre-equilibrated desalting column (PD-10, GE/Cytvia, 25 mM Tris, pH 7.4, 0.1 M KCl, 1 mM TCEP) to remove excess prCbl and concentrated via centrifugation in 25 mM Tris, pH 7.4, 0.1 M KCl, 1 mM TCEP to yield purified holo-*t*MS$^{HcyFolCob\ mut1•prCbl}$ (~15 mg/mL), which was stored at 4 °C or flash-frozen for long-term storage at -80 °C.

*t*MS$^{HcyFolCob\ mut2•aeCbl}$ (Hcy-on)

Purification of *t*MS$^{HcyFolCob\ mut2•aeCbl}$ was conducted similarly, with no added cobalamin. Protein purification yielded purified apo- of *t*MS$^{HcyFolCob\ mut2}$ (~20 mg/mL); to the purified apo protein (~150 µM) was added aminoethylcobalamin (aeCbl, ~170 µM). The resulting mixture was loaded onto a pre-equilibrated desalting column (PD-10, GE/Cytvia, 25 mM Tris, pH 7.4, 0.1 M KCl, 1 mM TCEP) to remove excess aeCbl and concentrated via centrifugation in 25 mM Tris,

pH 7.4, 0.1 M KCl, 1 mM TCEP to yield purified holo-*t*MS$^{\text{HcyFolCob mut2•aeCbl}}$, which was stored at 4 °C or flash-frozen for long-term storage at -80 °C.

_t_MS Qualitative UV-Vis Assay

The methylcobalamain:homocysteine methyltransferase reaction was monitored in the presence or absence of *t*MS constructs spectrophotometrically in the dark, tracking the time-dependent spectral changes of methylcobalamin (MeCbl) in the presence of homocysteine at 50˚C for up to 10 minutes. The assay was carried out under aerobic conditions for the qualitative examination. Time-dependent changes in absorbance of the mixture were recorded at 0 min (immediately after mixing), 5 min, and 10 min after adding homocysteine (final concentration of 100 μM). Both unbound/free MeCbl (20 μM) and protein-bound MeCbl (*t*MS$^{\text{CapCob}}$, 23 μM) were used as the methyl donors. Truncated *t*MS fragments, tMS$^{\Delta\text{N35Hcy}}$ and *t*MS$^{\text{HcyFol}}$, were used to catalyze the reaction (2 μM). The mixture containing Mecobalamin, *t*MS constructs (if applicable) were placed in 50 mM KPB pH 7.4, and 0.5 mM TCEP in a cuvette. The cuvette was incubated at 50 °C and the reaction was initiated by the addition of homocysteine (final concentration of 100 μM). The total volume of the reaction mixture was 1 mL. Spectral changes were recorded for up to 10 min using a Cary 300 Bio UV-Vis spectrophotometer (Varian, Inc.).

Crystallization of _t_MS Constructs

Crystals were grown via sitting drop vapor diffusion. *t*MS$^{\text{FolCob D759A•MeCbl}}$ (~10 mg/mL in 25 mM KPB, pH 7.4) was mixed with a reservoir solution containing 25% PEG 3350, 0.1 M Tris (pH 8.5), and 0.2 M ammonium acetate in a 1:1 ratio (0.4μL each) and incubated at 4˚C. Crystals were briefly transferred to a cryoprotectant solution containing approximately 20% glycerol and 20% PEG 3350, 0.08 M Tris (pH 8.5), and 0.16 M ammonium acetate for 30 seconds prior to harvesting and flash freezing in liquid nitrogen.

*t*MS$^{\text{FolCob D762G•cpCbl}}$ (~10 mg/mL in 25 mM KPB, pH 7.4) was mixed with a reservoir solution containing 1.26 M $(NH_4)_2SO_4$, 0.1M CHES-Na (pH 9.5), and 0.2 M NaCl in a 1:1 ratio (0.4 μL each) and incubated at 20˚C. Crystals were briefly transferred to a cryoprotectant solution containing approximately 20% glycerol and 1 M $(NH_4)_2SO_4$, 0.08 M CHES-Na (pH 9.5), and 0.16 M NaCl for 3 minutes prior to harvesting and flash freezing in liquid nitrogen.

*t*MS$^{\text{HcyFolCob mut1•prCbl}}$ (~15 mg/mL in 25 mM Tris, pH 7.5, 50 mM KCl, 1 mM TCEP) was mixed with a reservoir solution containing 30% PEG 3350, 0.1 M Bis-Tris (pH 6.5), and 0.2 M NaCl in a 1:1 ratio (0.4 μL each) and incubated at 20˚C. Crystals were briefly transferred to a cryoprotectant solution containing approximately 20% glycerol and 24 % PEG 3350, 0.08 M Bis-Tris (pH 6.5), and 0.16 M NaCl for ~30 seconds prior to harvesting and flash freezing in liquid nitrogen.

*t*MS$^{\text{HcyFolCob mut2•aeCbl}}$ (~18 mg/mL in 25 mM Tris, pH 7.5, 50 mM KCl, 1 mM TCEP) was mixed with a reservoir solution containing 20% PEG 3350, 0.1 M Tris (pH 8.5), and 0.2 M NaCl in a

1:1 ratio (0.4 μL each) and incubated at 4˚C. Crystals were briefly harvested and flash frozen in liquid nitrogen.

Data collection and processing statistics are summarized in Supplementary Table 1. Data for *t*MS$^{\text{FolCob D759A•MeCbl}}$ were indexed to spacegroup $P4_12_12$ (unit-cell parameters a = b = 187.77, c = 325.55 Å) with six molecules in the asymmetric unit (Matthew's coefficient VM = 4.22 Å3 Da−1, 71% solvent content). Data for *t*MS$^{\text{FolCob D762G•cpCbl}}$ were indexed to spacegroup $P6_122$ (unit-cell parameters a = b = 95.15, c = 274.29 Å) with one molecule in the asymmetric unit (Matthew's coefficient VM = 3.17 Å3 Da−1, 61% solvent content). Data for *t*MS$^{\text{HcyFolCob mut1•prCbl}}$ were indexed to spacegroup $P2_12_12_1$ (unit-cell parameters a = 69.95, b = 83.82, c = 163.72 Å) with one molecule in the asymmetric unit (Matthew's coefficient VM = 2.51 Å3 Da−1, 51% solvent content). Data for *t*MS$^{\text{HcyFolCob mut2•aeCbl}}$ were indexed to spacegroup $P2_12_12_1$ (unit-cell parameters a = 70.81, b = 115.10, c = 120.80 Å) with one molecule in the asymmetric unit (Matthew's coefficient VM = 2.58 Å3 Da−1, 52% solvent content).

Data Collection and Refinement

X-ray data sets were collected at 100 K on GM/CA beamline 23-ID-B at the Advanced Photon Source, Argonne National Laboratory (Argonne, IL) for *t*MS$^{\text{FolCob D759A•MeCbl}}$ and *t*MS$^{\text{FolCob D762G•cpCbl}}$, on GM/CA beamline 23-ID-D for *t*MS$^{\text{HcyFolCob mut2•aeCbl}}$, and on LS-CAT beamline 21-ID-D at the Advanced Photon Source, Argonne National Laboratory (Argonne, IL) for *t*MS$^{\text{HcyFolCob mut1•prCbl}}$. Data sets were processed using xia2/DIALS[44]. Initial phases were obtained using MOLREP[45]. Individual domains of the full-length *t*MS structure (8SSC) were used as search models. Iterative model building and corrections were performed manually using Coot[46] following molecular replacement and subsequent structure refinement was performed with CCP4 Refmac5[47]. Initial refinement was conducted using BUSTER[48] to rapidly fix Ramachandran, rotamer, and density fit outliers, refining to convergence and adding waters in the final automated round of refinement. Phenix eLBOW[49] was used to generate the initial ligand restraints using ligand ID "COB" or "B12". Phenix LigandFit[50] was used to provide initial fits and placements of the ligands. PDB-REDO[51] was used to assess the model quality in between refinements and to fix any rotamer and density fit outliers automatically. The model quality was evaluated using MolProbity[52]. The Hcy-on structure data set showed partial crystal twinning and final rounds of refinement were conducted using twin refinement, as suggested by PDB-REDO. Figures showing crystal structures were generated in PyMOL[53].

Statistical Analysis and Reproducibility

Unless otherwise stated, functional assays were conducted using n = 2 independent replicates. At least three independent experiments were conducted for each functional assay. All attempts at replication were successful. Analysis and curve-fitting was performed using Prism 10.2.3.

Data Availability

The structure coordinates and structure factors reported in this study have been deposited in the Protein Data Bank under accession codes 9CBO (*t*MS$^{\text{FolCob D759A•MeCbl}}$), 9CBP (*t*MS$^{\text{HcyFolCob mut1•prCbl}}$), 9CBQ (*t*MS$^{\text{FolCob D762G•cpCbl}}$), and 9CBR (*t*MS$^{\text{HcyFolCob mut2•aeCbl}}$). PDB codes of previously published structures used in this study are 8SSC, 8SSD, 8SSE, and 8G3H. All other data are available from the corresponding authors upon request. Source data are provided with this paper.

References

1. Matthews, R. G., Koutmos, M. & Datta, S. Cobalamin-dependent and cobamide-dependent methyltransferases. *Curr. Opin. Struct. Biol.* **18**, 658–666 (2008).
2. Banerjee, R. V. & Matthews, R. G. Cobalamin-dependent methionine synthase. *FASEB J.* **4**, 1450–1459 (1990).
3. Fujii, K. & Huennekens, F. M. Activation of Methionine Synthetase by a Reduced Triphosphopyridine Nucleotide-dependent Flavoprotein System. *J. Biol. Chem.* **249**, 6745–6753 (1974).
4. Banerjee, R. V., Harder, S. R., Ragsdale, S. W. & Matthews, R. G. Mechanism of reductive activation of cobalamin-dependent methionine synthase: an electron paramagnetic resonance spectroelectrochemical study. *Biochemistry* **29**, 1129–1135 (1990).
5. Brown, K. L. & Peck-Siler, S. Heteronuclear NMR studies of cobalamins. 9. Temperature-dependent NMR of organocobalt corrins enriched in carbon-13 in the organic ligand and the thermodynamics of the base-on/base-off reaction. *Inorg. Chem.* **27**, 3548–3555 (1988).
6. Datta, S., Koutmos, M., Pattridge, K. A., Ludwig, M. L. & Matthews, R. G. A disulfide-stabilized conformer of methionine synthase reveals an unexpected role for the histidine ligand of the cobalamin cofactor. *Proc. Natl. Acad. Sci.* **105**, 4115–4120 (2008).
7. Bandarian, V., Ludwig, M. L. & Matthews, R. G. Factors modulating conformational equilibria in large modular proteins: A case study with cobalamin-dependent methionine synthase. *Proc. Natl. Acad. Sci.* **100**, 8156–8163 (2003).
8. Jarrett, J. T., Huang, S. & Matthews, R. G. Methionine Synthase Exists in Two Distinct Conformations That Differ in Reactivity toward Methyltetrahydrofolate, Adenosylmethionine, and Flavodoxin†. *Biochemistry* **37**, 5372–5382 (1998).

9. Mendoza, J., Purchal, M., Yamada, K. & Koutmos, M. Structure of full-length cobalamin-dependent methionine synthase and cofactor loading captured in crystallo. *Nat. Commun.* **14**, 6365 (2023).
10. Drennan, C. L., Huang, S., Drummond, J. T., Matthews, R. G. & Ludwig, M. L. How a Protein Binds B_{12} : A 3.0 Å X-Ray Structure of B_{12} -Binding Domains of Methionine Synthase. *Science* **266**, 1669–1674 (1994).
11. Watkins, M. B., Wang, H., Burnim, A. & Ando, N. Conformational switching and flexibility in cobalamin-dependent methionine synthase studied by small-angle X-ray scattering and cryoelectron microscopy. *Proc. Natl. Acad. Sci.* **120**, e2302531120 (2023).
12. Taylor, R. T. & Weissbach, H. N^5-Methyltetrahydrofolate-homocysteine transmethylase: propylation characteristics with use of a chemical reducing system and purified enzyme. *J. Biol. Chem.* **242**, 1509–1516 (1967).
13. Fleischhacker, A. S. & Matthews, R. G. Ligand Trans Influence Governs Conformation in Cobalamin-Dependent Methionine Synthase. *Biochemistry* **46**, 12382–12392 (2007).
14. Bandarian, V., Ludwig, M. L. & Matthews, R. G. Factors modulating conformational equilibria in large modular proteins: A case study with cobalamin-dependent methionine synthase. *Proc. Natl. Acad. Sci.* **100**, 8156–8163 (2003).
15. Jarrett, J. T. *et al.* Mutations in the B12-Binding Region of Methionine Synthase: How the Protein Controls Methylcobalamin Reactivity. *Biochemistry* **35**, 2464–2475 (1996).
16. Bandarian, V. & Matthews, R. G. Measurement of Energetics of Conformational Change in Cobalamin-Dependent Methionine Synthase. in *Methods in Enzymology* vol. 380 152–169 (Academic Press, 2004).

17. Liptak, M. D., Fleischhacker, A. S., Matthews, R. G. & Brunold, T. C. Probing the Role of the Histidine 759 Ligand in Cobalamin-Dependent Methionine Synthase. *Biochemistry* **46**, 8024–8035 (2007).
18. Kung, Y. *et al.* Visualizing molecular juggling within a B12-dependent methyltransferase complex. *Nature* **484**, 265–269 (2012).
19. Zydowsky, T. M. *et al.* Stereochemical analysis of the methyl transfer catalyzed by cobalamin-dependent methionine synthase from Escherichia coli B. *J. Am. Chem. Soc.* **108**, 3152–3153 (1986).
20. Dorweiler, J. S., Finke, R. G. & Matthews, R. G. Cobalamin-Dependent Methionine Synthase: Probing the Role of the Axial Base in Catalysis of Methyl Transfer between Methyltetrahydrofolate and Exogenous Cob(I)alamin or Cob(I)inamide. *Biochemistry* **42**, 14653–14662 (2003).
21. Yamada, K. & Koutmos, M. The folate-binding module of Thermus thermophilus cobalamin-dependent methionine synthase displays a distinct variation of the classical TIM barrel: a TIM barrel with a `twist'. *Acta Crystallogr. Sect. Struct. Biol.* **74**, 41–51 (2018).
22. Koutmos, M., Datta, S., Pattridge, K. A., Smith, J. L. & Matthews, R. G. Insights into the reactivation of cobalamin-dependent methionine synthase. *Proc. Natl. Acad. Sci.* **106**, 18527–18532 (2009).
23. Bandarian, V. *et al.* Domain alternation switches B12-dependent methionine synthase to the activation conformation. *Nat. Struct. Biol.* **9**, 53–56 (2002).
24. Koutmos, M. *et al.* Metal active site elasticity linked to activation of homocysteine in methionine synthases. *Proc. Natl. Acad. Sci.* **105**, 3286–3291 (2008).

25. Matthews, R. G. *et al.* Cobalamin-Dependent and Cobalamin-Independent Methionine Synthases: Are There Two Solutions to the Same Chemical Problem? *Helv. Chim. Acta* **86**, 3939–3954 (2003).
26. Goulding, C. W., Postigo, D. & Matthews, R. G. Cobalamin-Dependent Methionine Synthase Is a Modular Protein with Distinct Regions for Binding Homocysteine, Methyltetrahydrofolate, Cobalamin, and Adenosylmethionine. *Biochemistry* **36**, 8082–8091 (1997).
27. Goulding, C. W. & Matthews, R. G. Cobalamin-Dependent Methionine Synthase from Escherichia coli: Involvement of Zinc in Homocysteine Activation. *Biochemistry* **36**, 15749–15757 (1997).
28. Banerjee, R. V., Frasca, V., Ballou, D. P. & Matthews, R. G. Participation of Cob(I)alamin in the reaction catalyzed by methionine synthase from Escherichia coli: a steady-state and rapid reaction kinetic analysis. *Biochemistry* **29**, 11101–11109 (1990).
29. Evans, J. C. *et al.* Structures of the N-terminal modules imply large domain motions during catalysis by methionine synthase. *Proc. Natl. Acad. Sci.* **101**, 3729–3736 (2004).
30. Koutmos, M. *et al.* Metal active site elasticity linked to activation of homocysteine in methionine synthases. *Proc. Natl. Acad. Sci.* **105**, 3286–3291 (2008).
31. Hagemeier, C. H., Křer, M., Thauer, R. K., Warkentin, E. & Ermler, U. Insight into the mechanism of biological methanol activation based on the crystal structure of the methanol-cobalamin methyltransferase complex. *Proc. Natl. Acad. Sci.* **103**, 18917–18922 (2006).
32. Seravalli, J., Brown, K. L. & Ragsdale, S. W. Acetyl Coenzyme A Synthesis from Unnatural Methylated Corrinoids: Requirement for "Base-Off" Coordination at Cobalt. *J. Am. Chem. Soc.* **123**, 1786–1787 (2001).

33. Svetlitchnaia, T., Svetlitchnyi, V., Meyer, O. & Dobbek, H. Structural insights into methyltransfer reactions of a corrinoid iron–sulfur protein involved in acetyl-CoA synthesis. *Proc. Natl. Acad. Sci.* **103**, 14331–14336 (2006).
34. Norris, P. R. & Pratt, J. M. Methyl transfer reactions of protein-free Co corrinoids. *BioFactors* **5**, 240–241 (1996).
35. Hogenkamp, H. P. C., Bratt, G. T. & Sun, S. Z. Methyl transfer from methylcobalamin to thiols. A reinvestigation. *Biochemistry* **24**, 6428–6432 (1985).
36. Galezowski, W. Methyl Transfer Reactivity of Five-Coordinate CH3CoIIIPc. *Inorg. Chem.* **44**, 1530–1546 (2005).
37. Seravalli, J., Brown, K. L. & Ragsdale, S. W. Acetyl Coenzyme A Synthesis from Unnatural Methylated Corrinoids: Requirement for "Base-Off" Coordination at Cobalt. *J. Am. Chem. Soc.* **123**, 1786–1787 (2001).
38. Smith, E. L., Mervyn, L., Johnson, A. W. & Shaw, N. Partial Synthesis of Vitamin B12 Coenzyme and Analogues. *Nature* **194**, 1175–1175 (1962).
39. Sato, K., Hiel, E. & Shimizu, S. Affinity chromatography of N 5-methyltetrahydropfolate-homocysteine methyltransferase on a cobalamin-sepharose. *FEBS Lett.* **85**, 73–76 (1978).
40. Yamada, K., Yamada, S., Tobimatsu, T. & Toraya, T. Heterologous High Level Expression, Purification, and Enzymological Properties of Recombinant Rat Cobalamin-dependent Methionine Synthase*. *J. Biol. Chem.* **274**, 35571–35576 (1999).
41. Structural genomics projects in Japan | Nature Structural & Molecular Biology. https://www.nature.com/articles/nsb1100_943.
42. Grabski, A., Mehler, M. & Drott, D. The Overnight Express Autoinduction System: High-density cell growth and protein expression while you sleep. *Nat. Methods* **2**, 233–235 (2005).

43. Studier, F. W. Protein production by auto-induction in high-density shaking cultures. *Protein Expr. Purif.* **41**, 207–234 (2005).
44. Winter, G. *et al.* DIALS: implementation and evaluation of a new integration package. *Acta Crystallogr. Sect. Struct. Biol.* **74**, 85–97 (2018).
45. Vagin, A. & Teplyakov, A. Molecular replacement with MOLREP. *Acta Crystallogr. D Biol. Crystallogr.* **66**, 22–25 (2010).
46. Emsley, P., Lohkamp, B., Scott, W. G. & Cowtan, K. Features and development of Coot. *Acta Crystallogr. D Biol. Crystallogr.* **66**, 486–501 (2010).
47. Murshudov, G. N. *et al.* REFMAC5 for the refinement of macromolecular crystal structures. *Acta Crystallogr. D Biol. Crystallogr.* **67**, 355–367 (2011).
48. Smart, O. S. *et al.* Exploiting structure similarity in refinement: automated NCS and target-structure restraints in BUSTER. *Acta Crystallogr. D Biol. Crystallogr.* **68**, 368–380 (2012).
49. Moriarty, N. W., Grosse-Kunstleve, R. W. & Adams, P. D. electronic Ligand Builder and Optimization Workbench (eLBOW): a tool for ligand coordinate and restraint generation. *Acta Crystallogr. D Biol. Crystallogr.* **65**, 1074–1080 (2009).
50. Terwilliger, T. C., Klei, H., Adams, P. D., Moriarty, N. W. & Cohn, J. D. Automated ligand fitting by core-fragment fitting and extension into density. *Acta Crystallogr. D Biol. Crystallogr.* **62**, 915–922 (2006).
51. Joosten, R. P., Long, F., Murshudov, G. N. & Perrakis, A. The PDB_REDO server for macromolecular structure model optimization. *IUCrJ* **1**, 213–220 (2014).
52. Chen, V. B. *et al.* MolProbity: all-atom structure validation for macromolecular crystallography. *Acta Crystallogr. D Biol. Crystallogr.* **66**, 12–21 (2010).
53. Schrödinger, LLC. The PyMOL Molecular Graphics System, Version 2.5.4 (2021).